JOURNAL OF GEOPHYSICAL RESEARCH, VOL. 103, NO. D18, PAGES 23,207-23,216, SEPTEMBER 27, 1998

Cirrus layer microphysical properties derived from surface-based millimeter radar and infrared interferometer data

Gerald G. Mace

Department of Meteorology, University of Utah, Salt Lake City

Thomas P. Ackerman

Department of Meteorology, Pennsylvania State University, University park

Patrick Minnis and David F. Young

Atmospheric Sciences Division, NASA, Langley Research Center, Hampton

Abstract. Observational data regarding the properties of cirrus clouds are needed to aid in the development of accurate, physically based parameterizations in climate models. The Atmospheric Radiation Measurement (ARM) program, sponsored by the U.S. Department of Energy, is providing continuous observations of cirrus clouds with a suite of instrumentation at several locales. In this paper, we describe an algorithm to derive the microphysical properties of optically thin cirrus clouds. This algorithm uses radar reflectivity and infrared emission spectra from an interferometer and is tailored for the specific instruments at the ARM sites. We present in situ validation of the technique and examine a cirrus case study to illustrate the sensitivity of the algorithm. In the case study, solar fluxes calculated from the retrieved microphysical parameters are compared to observed fluxes to build confidence in the algorithm results. Comparison of the retrieved quantities to microphysical parameters retrieved from satellite data is also presented.

1. Introduction

Because of their frequency of occurrence and location in the cold upper troposphere, cirrus clouds are an integral component of the global climate system. These clouds, composed of ice crystals of variable habit [*Dowling and Radke*, 1990], form in association with many atmospheric dynamical processes such as jet streams, frontal systems and deep convection [*Liou*, 1986] and often demonstrate organization on mesoscale to synoptic spatial and temporal scales [*Starr and Wylie*, 1990; *Mace et al.*, 1995]. Since sublimation of cirrus crystals is a slow process relative to the evaporation of cloud water droplets and crystal terminal velocities tend to be substantial (~1 m s^{-1}), cirrus can perturb diabatic heating rates many kilometers below and tens to even hundreds of kilometers downstream of the primary generation region.

While it is certain that cirrus are important to the global climate, the nature of this effect has been a topic of scientific research for more than two decades. Studies have shown that the effect of the infrared greenhouse due to cirrus (warming) dominates over the effect of the cirrus on the solar radiation (cooling) in situations where the clouds are optically thin and occur over a warm surface [e.g., *Ackerman et al.*, 1988]. This effect tends to reverse as cloud optical thickness increases. *Stephens et al.* [1990] showed, however, that these effects are strongly modulated by the microphysical properties of the cloud. Whatever the sign of the radiative effect, modeling studies have shown that the atmospheric general circulation is very sensitive to cirrus occurrence and cirrus properties [*Lohman and Roeckner*, 1995].

Given the sensitivity of the global climate to cirrus, it is important that global climate models used to simulate climate and climate change correctly incorporate the effects of cirrus. However, given the extreme variability of cirrus microphysical properties [*Dowling and Radke*, 1990] and the complex interaction between solar radiation and the nonspherical particles composing cirrus clouds [*Takano and Liou*, 1989], it is a virtual certainty that current climate models do not treat cirrus correctly. As a result, the calculated response of climate models to changes in cirrus properties are certainly questionable. This, in turn, impacts their sensitivity to changes in internal and external forcing.

A number of issues can be raised pertaining to the shortcomings of cirrus parameterizations in climate models. However, the principal shortcoming rests largely with a paucity

Paper number 98JD02117.
0148-0227/98/98JD-02117$09.00

of observational data that relate cirrus macrophysical, microphysical, and radiative properties to the atmospheric state resolved by a large-scale model. While a number of intensive observing programs directed at cirrus have been conducted in the last decade and the results emanating from these studies have greatly increased our knowledge, those results represent a few instantaneous samples in a broadly distributed continuum and, thus, have somewhat limited applicability to parameterizing cirrus in climate models. The broad gaps in the observational database can be treated in a number of ways. Perhaps the most obvious approach would be to combine cloud properties retrieved from satellite data [*Minnis et al.* 1993a; *Wylie and Menzel*, 1989] with meteorological data from observational models. A second approach is to instrument very heavily a number of surface sites strategically located in climatically significant regimes and to record data continuously for many years. This latter approach has been adopted by the Department of Energy (DOE) Atmospheric Radiation Measurement (ARM) program [*Stokes and Schwartz*, 1994].

In anticipation of the installation of an operational cloud radar at the southern great plains (SGP) ARM site, *Mace et al.* [1997] examined cirrus cloud properties derived from a 3 month cloud radar data set observed by the Penn State 94 GHz cloud radar. While this study revealed a number of interesting results, it was limited by the short duration of the data set and a lack of supporting observations. The cloud radar at the SGP site provides an opportunity to extend this methodology to longer time periods and to examine a wider range of parameters. However, to compile statistics of cirrus microphysical properties and examine relationships between cloud properties and meteorological variables, algorithms must be implemented that combine remote sensing observations to retrieve the cloud properties of interest. In this paper, we describe one such algorithm that is being implemented operationally on the ARM data streams and present a comparison of the results of the algorithm with in situ data. A cirrus case study is also examined to illustrate the response of the retrieval algorithm to a cirrus event that persists for several hours over the SGP site

2. Algorithm Description

A number of algorithms have been published recently which combine radar reflectivity observations with downwelling infrared radiances to derive cirrus cloud microphysical properties [*Matrosov et al.*, 1992, 1994; hereinafter referred to as M92 and M94, respectively). The technique of M94 is an extension of M92 and retrieves ice water content (IWC) and characteristic particle size in each radar range gate by applying a statistical technique to deconvolve the Doppler velocity into mean air motions and particle terminal velocities. Our approach is to use the general ideas of M92 and calculate the layer-averaged properties of optically thin cirrus using the particular mix of observational platforms at the ARM sites. For instance M92 and M94 use a narrow filed of view infrared radiometer that has a relatively rapid response (~30 s) and wide spectral band pass (9.94-11.43 μm). No such instrument suitable for cirrus observations is currently operational at the ARM sites. Therefore we use, for the first time, infrared radiance spectra observed by the atmospheric emittance radiance interferometer (AERI) [*Smith et al.*, 1993] combined with radar reflectivity observations to derive the microphysical properties of cirrus layers. We also seek to incorporate into the algorithm research results that were not available to M92.

Our initial goal is to derive accurate layer-averaged cloud properties to evaluate the effect of optically thin cirrus on the radiation field at the surface and top of atmosphere. Since the vertically resolved technique of M94 requires the deconvolution of the Doppler velocities, the M94 technique requires a rather homogeneous cirrus layer that persists for several hours; the techniques for deriving layer-averaged properties have no such requirement and are therefore more generally applicable. The approach discussed in this paper is also described briefly by *Mace et al.* [1998] as part of the Subsonic Aircraft: Contrails and Clouds Effects Special Study (SUCCESS) section in *Geophysical Research Letters*. In the following, we expand on *Mace et al.* [1998] and present additional results.

The primary assumption we employ is that the layer-mean particle size distribution (PSD) can be described adequately by a modified gamma function [*Dowling and Radke*, 1990] in the form presented by *Gossard* [1994]:

$$N(D) = \beta\left(\frac{D}{D_g}\right)^{\alpha} \exp\left[-\left(\frac{D-D_g}{D_g}\right)\right] \tag{1}$$

where β is a constant of proportionality, D_g is a length parameter, and α is the order of the distribution. We express this function in terms of the modal diameter by solving $\partial N(D)/\partial D=0$ for D_g, substitute the result into equation (1) and solve for β. The resulting equation is

$$N(D) = N_x \exp(\alpha)\left(\frac{D}{D_x}\right)\exp\left[-\frac{D\alpha}{D_x}\right] \tag{2}$$

where D_x is the modal diameter and N_x is the number of particles per unit volume per unit length at the functional maximum. Analysis of in situ data [*Dowling and Radke*, 1990] suggests that for cirrus $\alpha \leq 2$. We therefore set α=1 and use observations to estimate D_x and N_x.

A radar measures the backscatter cross section per unit volume, and this cross section can be expressed in terms of the liquid equivalent radar reflectivity factor Z_e. Assuming the Rayleigh approximation is valid [*Schneider and Stephens*, 1995] and neglecting differences in the refractive indexes of ice and water for the moment, Z_e is identical to the radar reflectivity factor

$$Z = \int_0^{\infty} N(D) D^6 dD\,. \tag{3}$$

By using (2) in (3), we can write

$$Z = N_x e^{\alpha} D_x^7 \frac{(6+\alpha)!}{\alpha^{7+\alpha}}\,. \tag{4}$$

Similarly, the water content can be expressed in terms of (2);

$$IWC = \rho_i \frac{\pi}{6} N_x D_x^7\,. \tag{5}$$

Using (4) in (5) we can write,

$$IWP = \overline{(IWC)}\Delta h = \rho_i \frac{\pi}{6} \overline{Z} \frac{\alpha^3}{D_x^3} \frac{(3+\alpha)!}{(6+\alpha)!}\Delta h \tag{6}$$

where IWP is the ice water path, Δh is the layer thickness and the overbars represent layer averages. Other parameters of interest can be derived similarly. For instance, the layer-mean

total particle concentration (N_T) and the effective spherical radius (r_e; defined in terms of the total volume of the distribution to the total area) can be written as

$$N_T = D_x N_x e^{\alpha} \frac{\alpha}{\alpha^{\alpha+1}}$$

$$r_e = \frac{D_x}{2} \frac{(3+\alpha)!}{(2+\alpha)!} \alpha^{\alpha} \quad (7)$$

The two unknown parameters of the modified gamma distribution can be determined from the observed downwelling radiance and the radar reflectivity using an expression for the layer emittance

$$\varepsilon = 1 - \exp\left[-(1-\bar{\omega}_0)\bar{\beta}\Delta h\right]. \quad (8)$$

In equation (8), ε is the cloud layer emittance, $\bar{\omega}_0$ is the single-scatter albedo, and β is the extinction coefficient. *Fu and Liou* [1993, hereinafter referred to as FL93] present third-order polynomial expressions for ω_0 and β in terms of an effective size, D_e and IWC. The FL93 D_e is the equivalent width of a distribution of hexagonal columns. Since we are formulating the retrieval in terms of spherical particles, we use regression analysis and the aspect ratios of *Auer and Veal* [1970] to recast the FL93 parameterization in terms of the radius that hexagonal columns would have if converted to spheres [*Ebert and Curry*, 1992]. This relationship takes the form

$$D_e = \sum_{i=0}^{i=4} C_i r_e^i \quad (9)$$

and is shown in Figure 1. The constants C_n of Equation 9 are listed in Table 1. The expression for ω_0 and β are then written in terms of r_e as in FL93,

$$\beta = \mathrm{IWC} \sum_{n=0}^{2} \frac{a_n}{r_e^n} \qquad 1-\omega_0 = \sum_{n=0}^{3} b_n r_e^n .$$

a_n and b_n are listed in Table 2. These results are substituted into equation 8 which takes the form,

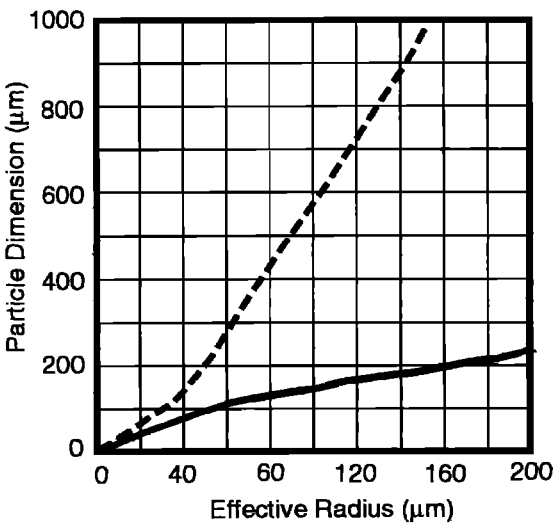

Figure 1. Particle maximum dimension (dashed) and particle width as a function of effective radius. Relationships assume hexagonal ice crystals and the aspect ratios of *Auer and Veal* [1970]

Table 1. Constants of Polynomial Expression Relating D_e and r_e.

	Coefficients
C_0	-1.0615×10^{1}
C_1	3.2419×10^{-0}
C_2	-2.197×10^{-2}
C_3	6.515×10^{-5}

$$ln(1-\varepsilon) = -\mathrm{IWC}\left(C_1 r_e^3 + C_2 r_e^2 + C_3 r + C_5 r_e^{-1} + C_6 r_e^{-2}\right)\Delta h \quad (10)$$

The constants C_n depend on a_n and b_n:

$$C_1 = a_0 b_3$$
$$C_2 = a_0 b_2 + a_1 b_3$$
$$C_3 = a_0 b_1 + a_1 b_2 + a_2 b_3$$
$$C_4 = a_0 b_0 + a_1 b_1 + a_2 b_2$$
$$C_5 = a_1 b_0 + a_1 b_1$$
$$C_6 = a_2 b_0 .$$

Before deriving an expression for the layer emittance in terms of Z_e and D_x, two other factors that influence the relationship must be considered. The effective density of ice crystals has been shown to be a strong function of particle size due to internal air pockets that form during crystal growth [*Brown and Francis*, 1995]. We use the parameterization presented by *Brown and Francis* [1995], equation (8), and the aspect ratios of *Auer and Veal* [1970] to develop a relationship for the bulk density of low-order, modified gamma distributions of ice crystals in terms of r_e. The parameterized relationship takes the form,

$$\rho_{i,eff} = \sum_{n=0}^{n=3} \frac{B_n}{r_e^n} \quad (11)$$

and is shown in Figure 2 for α=1. The constants B_n are listed in Table 3. The departure of bulk density from solid ice also affects the radar reflectivity through the refractive index [*Atlas et al.*, 1995]. We therefore adopt the approach outlined by *Atlas et al.* [1995] to express Z_e in terms of a distribution of ice spheres that obey the bulk density formulation of equation (11). This allows us to write equation (5) as follows:

$$\overline{\mathrm{IWC}} = \frac{Z_e}{D_x^3} \frac{\rho_{i,eff}^2}{\rho_{i,solid}} \left(\frac{K_i}{K_w}\right)^2 \frac{\pi}{6} \alpha^3 \frac{(3+\alpha)!}{(6+\alpha)!} \quad (12)$$

Finally, we use equations (11), (12), and (7) in equation (10) to express D_x in terms of the layer emittance and layer-mean radar reflectivity,

Table 2. Constants of Polynomial Expressions Relating β and r_e (a_n) and ω_0 and r_e (b_n)

	9.1-10.2 μm	10.2-12.5 μm
a_0	$+0.3217 \times 10^{-2}$	$+0.5108 \times 10^{-2}$
a_1	$+0.1707 \times 10^{+1}$	$+0.1067 \times 10^{+1}$
a_2	$+0.1105 \times 10^{+2}$	$+0.7083 \times 10^{+1}$
b_0	$+0.2595 \times 10^{0}$	$+0.5517 \times 10^{0}$
b_1	$+0.7275 \times 10^{-2}$	-0.2667×10^{-2}
b_2	-0.8006×10^{-4}	$+0.3021 \times 10^{-4}$
b_3	$+0.2453 \times 10^{-6}$	-0.9306×10^{-7}

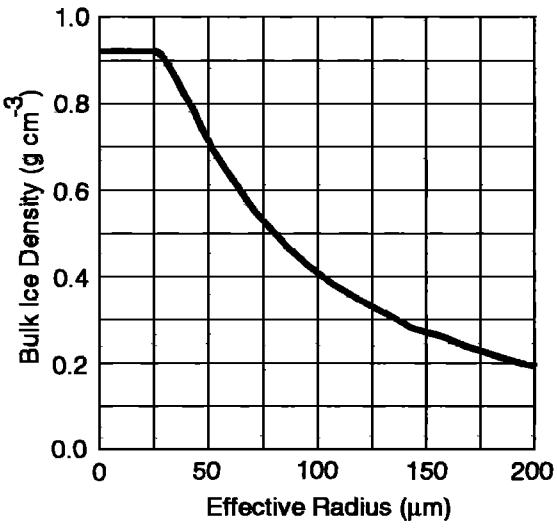

Figure 2. Relationship between effective radius and the bulk density of a first-order modified gamma distribution of ice crystals

$$\frac{\ln(1-\varepsilon)}{k_1 \bar{Z}_e \Delta h} = \frac{C_1 k_2^3 D_x^5 + C_2 k_2^2 D_x^4 + C_3 k_2 D_x^3 + C_4 D_x^2 + \frac{C_5}{k_2} D_x + \frac{C_6}{k_2^2}}{D_x^2 \left(B_0 D_x^3 + \frac{B_1}{k_2} D_x^2 + \frac{B_2}{k_2^2} D_x + \frac{B_3}{k_2^3} \right)} \quad (13)$$

where

$$k_1 = \left(\frac{k_i^2}{k_w^2} \right) \rho_{i,solid}^2 \frac{\pi}{6} \alpha^3 \frac{(3+\alpha)!}{(6+\alpha)!}$$

$$k_2 = \frac{1}{2} \frac{(3+\alpha)!}{(2+\alpha)!} \frac{1}{\alpha^2}.$$

Using the observed reflectivity and the layer emittance determined from the downwelling radiance as described below, equation (13) is solved numerically for D_x, and D_x is used in equation (4) to determine N_x.

The response of equation (12) to typical values of emittance and radar reflectivity is shown in Figure 3. It is encouraging to note that the retrieved parameters depend to a nearly equal degree on the input parameters, and the retrieval results tend to remain within the ranges typical of cirrus [*Dowling and Radke*, 1990]. For a given radar reflectivity the water content, number concentration, and visible optical depth increase while the effective size decreases for increasing beam emittance. Holding the beam emittance constant, all parameters increase with increasing radar reflectivity. This is especially notable for particle size, which is, as expected, somewhat more sensitive to the radar reflectivity than to beam emittance. This figure also suggests that the visible optical depth and water content are most sensitive to observational error at larger values of reflectivity and beam emittance, while effective size is most sensitive to error at the larger particle sizes.

Table 3. Constants of Polynomial Expression Relating $\rho_{I,eff}$ and r_e.

	Coefficients
B_0	-0.7076×10^{-1}
B_1	$+0.5775 \times 10^{+2}$
B_2	$-0.1078 \times 10^{+4}$
B_3	$+0.6396 \times 10^{+4}$

The infrared emittance of an optically thin cirrus layer must be computed in order to implement equation (13). The primary observation used to determine ε is the downwelling radiance measured by the AERI. The AERI is a zenith-viewing instrument that measures the downwelling radiance in a 1.3° field of view at 0.5 cm^{-1} spectral resolution. The instrument provides an emission spectrum valid over a 3 min atmospheric dwell time once every 8 min. We consider the spectral region between 800 and 1000 cm^{-1} and average the 0.5 cm^{-1} observations to 5 cm^{-1} to reduce uncertainty in the observations. We use the intervals that contain no significant gaseous emission lines in calculating ε. Our ability to choose well-characterized narrow spectral bands is a distinct advantage of using the AERI. Narrow field of view radiometers, as used by M92, have relatively wide spectral band passes and are therefore quite sensitive to uncertainties due to trace gas emission. Since scattering of IR radiation from the cloud and surface cannot be neglected in determining ε [*Platt and Stephens*, 1980], we have developed an iterative approach based on the MODTRAN3 radiance algorithm [*Berk et al.*, 1989] which includes a multiple-scattering implementation of the DISORT program [*Stamnes et al.*, 1988].

We first identify a period when no clouds are present in the AERI field of view that is temporally near the cirrus cloud event. Using a radiosonde profile, we then calculate the downwelling radiances in 5 cm^{-1} intervals between 800 and 1000 cm^{-1}. The clear sky calculations are compared to the AERI observations at the clear time, and those wavenumber bins that can be modeled accurately (to within 10% of the observed radiance) are used in the retrieval. Typically, several dozen spectral intervals are used. Since the AERI is believed accurate to within 0.5% [*Smith et al.*, 1993], errors in the clear sky calculation are due to errors in the MODTRAN spectroscopic database or to errors in the thermodynamic profile. A correction factor for each spectral interval is then determined following *Smith et al.* [1993]. If the calculated clear sky radiances at the clear time and the cirrus time differ by more than one tenth of the clear sky offset we do not perform the retrieval unless the radiance observed at the cirrus time is more than 100% greater than the cirrus time calculated clear radiance corrected by the clear sky offset.

To perform the retrieval, we require that cirrus be present over the instrument, as determined by the radar, during the entire dwell time of the AERI. For a particular AERI observation containing cirrus, the radar reflectivity is corrected for gaseous attenuation by water vapor and oxygen using the algorithm of *Schroeder and Westwater* [1991] and are then averaged temporally and vertically through the depth of the cloud layer. In the first iteration, ε is specified to 0.5, and equation (13) is solved in each spectral interval. The ice water path and particle size are calculated using equations (5) and (6) and the IR single-scattering properties of the layer are determined in each spectral interval using the FL93 parameterization. The single-scattering properties are used as input to the MODTRAN3 algorithm, and the downwelling radiance in each spectral bin is computed and then compared to the observations. On the basis of the comparison, ε is adjusted, and the process is repeated using the adjusted ε. The iteration continues until the radiance averaged over the spectral bins converges on the observations. The number of iterations required for convergence depends on the radar reflectivity and

the amount the cirrus increase the downwelling radiance over the calculated clear sky amount. The algorithm typically converges in fewer than five iterations for cirrus that have a significant layer-mean reflectivity (> -30 dBZe) and radiance at least twice the calculated clear sky value. Occasionally, the algorithm does not converge for very tenuous cirrus.

This procedure results in individual retrievals in each spectral interval, and the individual retrievals generally agree to within 10% for cirrus layer parameters such as water path and effective particle size. The differences in the spectral retrievals are most likely due to the coarse spectral resolution of the FL93 parameterization in the thermal infrared portion of the spectrum. The reported properties of the cloud are taken to be the average of the individual retrievals. Since the AERI observations are valid over a period of time (~3 min) that may be long with respect to changes in the cloud properties, we perform the retrieval several times using the standard deviations of the AERI radiance and radar reflectivity added and subtracted to the temporally averaged radiance and radar reflectivity, respectively. The results of the four extreme permutations of the mean case are taken to be the observational uncertainty of the spectrally and temporally averaged retrieval. M94 present additional analyses of sensitivity for radar-radiometer retrievals in cirrus clouds.

3. Case Study Results

3.1 April 24, 1997

Since we retrieve layer-mean quantities with the algorithm described above, in situ validation requires representative cirrus microphysical observations averaged over an entire cirrus layer. On April 24, 1996, the NASA DC8, based in Salina, Kansas, as part of SUCCESS deployment, conducted a mission over the SGP site and performed a slow spiral descent through a uniform cirrus layer. This case is described in more detail by *Mace et al.* [1998]. Figure 4 shows the results of the comparison between the particle size distribution observed by the Particle Measurement Systems 2DC microphysical probe with the results of the retrieval algorithm described above. In the retrieval we assume the order of the modified gamma distribution to be unity and integrate the retrieved distribution over the 2DC size bins after converting the equivalent spherical radii to the maximum dimension of hexagonal columns using equation (8) and the aspect ratios of *Auer and Veal* [1970]. In the smallest size range (10-100 μm) the 2DC reported no particles, while the retrieval results suggest concentrations near 200 L^{-1}. Between 100 and 200 μm, the 2DC reports concentrations near 180 L^{-1}, while the

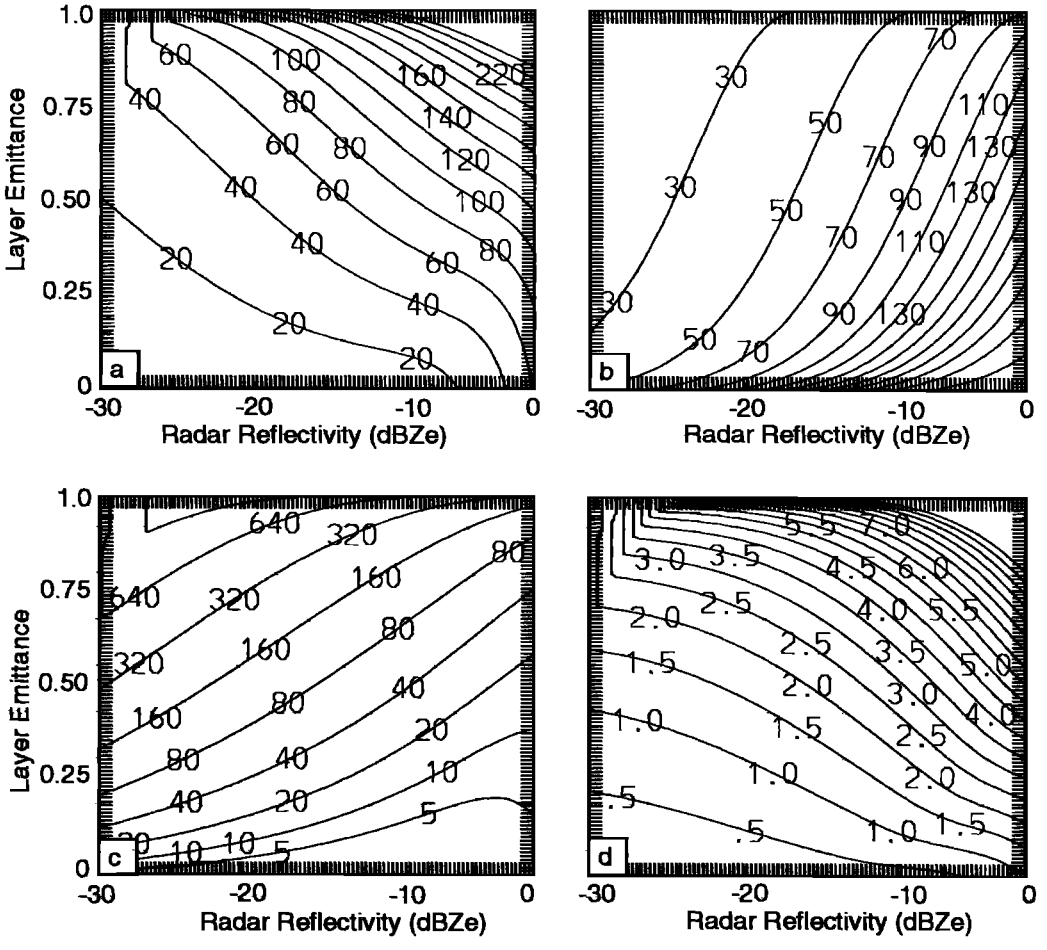

Figure 3. Response of the reflectivity-radiance algorithm to typical values of layer emittance and radar reflectivity. The assumed cloud depth is 1 km. (a) Layer-mean ice water content (mg m^{-3}). (b) Effective radius (μm). (c) Particle concentration (l^{-1}). (d) Visible optical depth derived from the *Fu and Liou* [1993] parameterization using the water content and effective size as input.

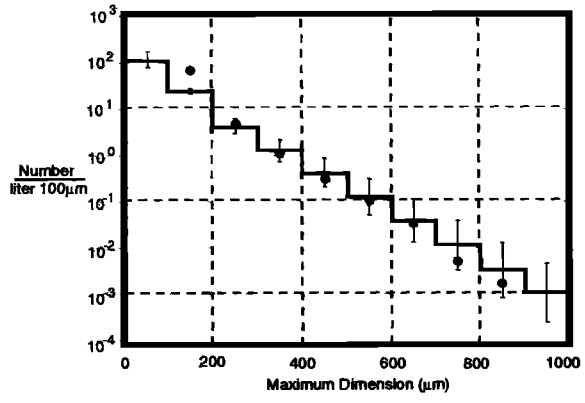

Figure 4. Comparison between the retrieved particle size distribution using the reflectivity-radiance algorithm discussed in the text and the measurements made by the 2DC microphysical probe on the NASA DC-8. The solid line shows the retrieved distribution, and the error bars are calculated from the standard deviations of the radiance and radar reflectivity during the retrieval period. The 2DC measurements are shown by the dot.

retrieval results are somewhat lower. In the remaining size bins, however, the agreement between the 2DC and the retrieval is quite good and remains within the range of the observational uncertainty of the retrieval results. The slope of the observed distribution is somewhat greater than the retrieved distribution and suggests that α slightly less than 1 may be more valid for this case.

Two explanations are possible for the discrepancy at the smallest two size bins. Since the radar responds to the sixth moment of the particle distribution and the radiance depends, to first order, on the integrated ice mass (third moment of the distribution), we are particularly insensitive to the smallest particles. We thus rely on the distribution of the larger particles to predict the distribution of the smaller. Our analysis has shown that for typical cirrus particle distributions, the bulk of the radar reflectivity is contributed by particles with effective radii between 80 and 200 μm. Therefore the retrieval accuracy of the smallest size particles depends on the correlative relationship between the larger and the smaller particles. Analysis of microphysical probe data has shown that this relationship is often tenuous; bimodal distributions are frequently observed, in which case there may be no relationship. Since we are effectively integrating over the depth of the layer, however, it is possible that these phenomena will be less important for layer averages. Further analysis is required to confirm this speculation.

An alternative explanation to the discrepancy in the smallest bins is related to the well-known difficulty of the 2DC to accurately observe the smaller end of the particle distribution. Since the 2DC observed no particles between 10 and 100 μm and, relative to the retrieval, counts too many particles in the 100-200 μm bin, it is possible that some of the smaller particles have been improperly counted in the larger bin. Certainly, additional analysis is required to confirm both of these possibilities, and it is likely that the discrepancy results from some combination of both effects. The overall agreement shown in Figure 4 is, however, quite encouraging. In the following section we explore an alternative means to validating the retrieval by comparing the observed solar flux at the surface with the solar flux calculated from the retrieved layer properties. Since the visible extinction is sensitive to the presence of smaller particles [*Ramaswamy and Detwiler*, 1986], the comparison allows us to gauge the overall accuracy of the technique for the case we consider.

3.2 April 5, 1997

The algorithm described in section 2 has been designed for operational implementation at the DOE ARM sites so that the layer-averaged microphysical properties of optically thin cirrus layers can be monitored continuously. While comparison of the retrieved results with in situ data is the preferred means of validation, in situ data are available only during infrequent intensive observing periods. Given the known variability of cirrus properties, it would be incorrect to assume that sporadic validation with in situ data confirms the validity of our results over the broad continuum of cirrus characteristics that will certainly be observed. We therefore investigate means by which individual cases can be examined independently and some measure of confidence in the retrieval results determined. Since the ultimate goal of this undertaking is the characterization of the effect of thin cirrus on the radiation field, we attempt to use the observed radiation field to validate the results. Since the cirrus-layer properties derived from the retrieval algorithm are guaranteed to produce the correct downwelling radiance in the thermal infrared portion of the spectrum, we compare, when possible, the downwelling solar flux observed at the surface with calculations of the solar flux which use the derived microphysical properties as inputs to radiative parameterizations. We also compare the retrieval results with those calculated from geostationary satellite observations. If we can show that the retrieved cloud properties lead to reasonable estimates of the solar flux at the surface and compare well with cloud properties derived from top of atmosphere radiances, then we can be confident that our results attain a sufficient level of accuracy.

In this section we present results from a cirrus event that occurred at the SGP site on April 5, 1996. While this is an interesting cirrus event in its own right, we use this case as an illustration of the products that will be generated operationally and the techniques we will use to validate the results. The cirrus shield that formed over the SGP site on April 5 occurred in association with a vigorous low-pressure system centered over southwest Texas. After middle and low-level cloudiness cleared just before 1800 UTC, an overcast cirrus layer persisted for many hours and during this time appeared visually to be quite uniform; very little horizontal structure in the overcast was apparent to ground observers. The radar reflectivity observed by the Pennsylvania State University 94 GHz cloud radar [*Clothiaux et al.*, 1995] confirms this observation (Plate 1a). While structure is evident in the time-height cross section, this structure evolved over temporal periods of 30 minutes to an hour. Before 2100 UTC, cloud base remained near 6.5 km, while radar cloud top was more variable and ranged between 8.5 and 10 km. After 2100 UTC, the layer thinned considerably and the layer-mean reflectivity decreased. These features, evident in the reflectivity cross section, can also be identified in the 11 μm radiance time series from the AERI (Plate 1b). For instance, the minima in radiance near 1900 UTC and 1945 UTC occur in conjunction with decreases in the reflectivity. During these radiance minima, the peak reflectivity values drop from peaks

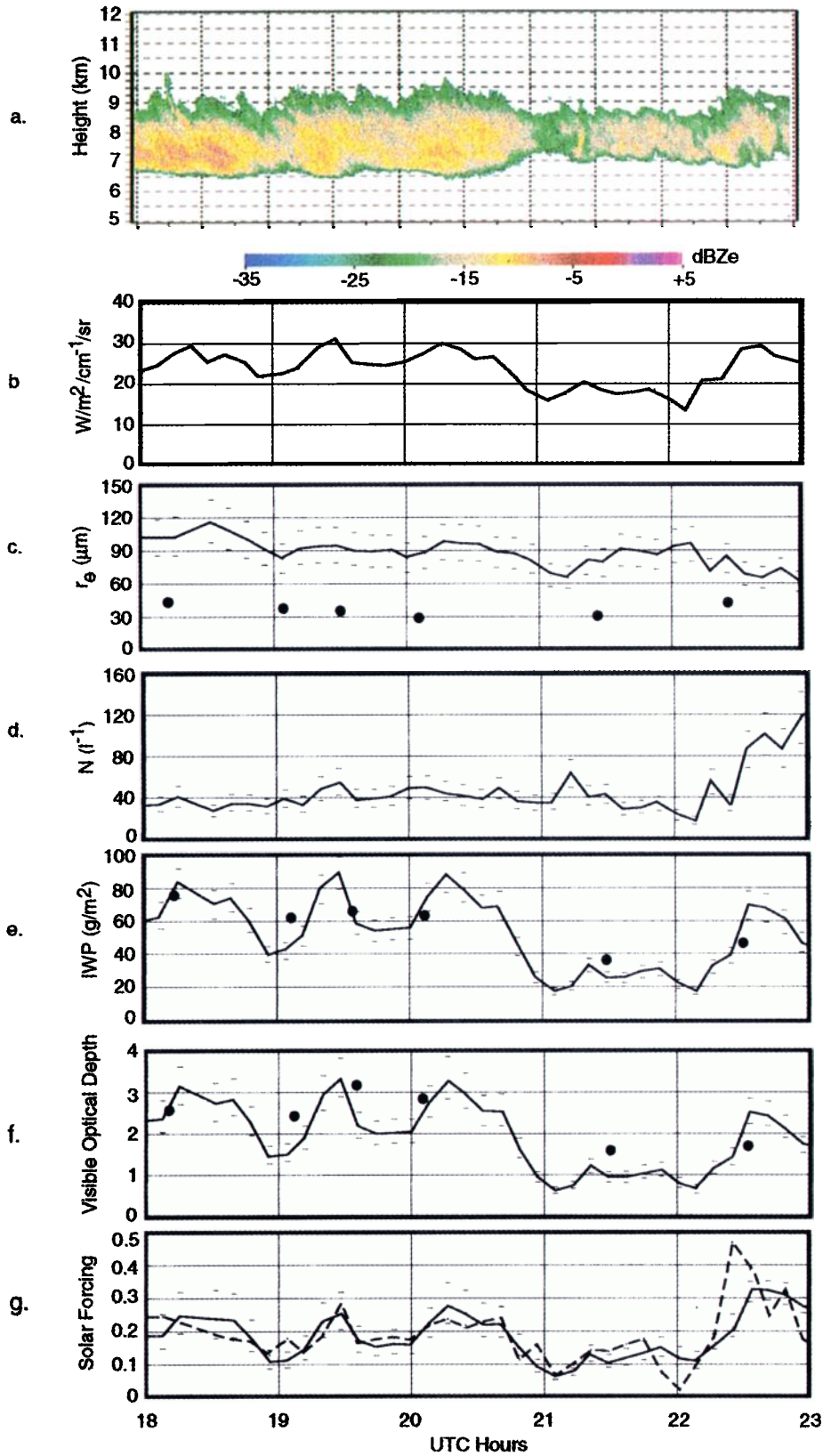

Plate 1. April 5, 1996, case study. The overcast cirrus deck was observed at the Southern Great Plains Atmospheric Radiation Measurement (SGP ARM) site in north central Oklahoma. (c-g) Solid lines show results from the radar-radiance algorithm, the horizontal tick marks show the uncertainty determined from the standard deviations of the radar reflectivity and atmospheric emitted radiance interferometer (AERI) radiance, and the circles show results derived from geostationary satellite radiances. (a) Time-height section of radar reflectivity observed by the PSU 94 GHz radar, (b) 11 μm radiance measured by the AERI, (c) Effective radius, (d) Retrieved particle concentration, (e) Ice water path, (f) Visible optical depth, and (g) Comparison of the observed solar flux (dashed line) with the solar flux calculated using the retrieval results in Plates 1e and 1c. The flux is expressed as the fraction of the clear sky flux removed by the cloud layer.

near -3 dBZe at 1835 and 1925 UTC to values near -15 dBZe. The 11μm radiance decreases substantially when the cloud thins after 21 UTC. Note, however, that between 2200 and 2300 UTC, the character of the cloud layer changes. During this time the radiance increases to values observed during the thicker and more radar-reflective periods observed earlier in the period, while the radar reflectivity between 2200 and 2300 UTC does not show a corresponding increase. The peak radar reflectivity values remain at or below -15 dBZe. The only notable change in the radar data during this hour is a thickening of the cloud layer from approximately x during the previous hour to x between 2200 and 2300 UTC.

Retrieved particle size, concentration and ice water path are shown in Plates 1c and 1d. For the purpose of discussion, we divide the case into three sections based on the changing layer thickness. From 1800 UTC until approximately 2030 UTC the layer maintains a thickness of 2.5-3 km, and from near 2100 UTC until 2215 UTC the layer thickness decreases to 1.5-2km. During the final period, 2230-2300, the layer thickness increases to approximately 2.5 km. During these periods the variations in the IWP correspond roughly to changes in the layer-averaged ice water content since layer thickness remains roughly constant. Ice water paths during the early period (1800-2030 UTC) are quite variable and range from 40-90 g m^{-2}, and the variability in the ice water path follows closely the evolution of the reflectivity and radiance. Water paths during the middle period (21-2215 UTC) decrease markedly. This decrease appears to be due, primarily, to a decrease in the layer thickness. Effective particle sizes range from near 120 μm during the early period maximum in reflectivity to approximately 70 μm at 2115 UTC during a local minimum in IWP. Particle concentrations during the early and middle periods are fairly steady and range between 30 and 60 L^{-1}.

The final 30 min period is characterized by smaller particles and much higher concentrations relative to the earlier times. While sizes decrease to about 60 μm during this time, concentrations increase by nearly a factor of 5 from 25 L^{-1} at 2215 UTC to 120 L^{-1} at 2300 UTC. The average reflectivity of the layer increases only slightly during this time, however, the downwelling radiance doubles from 15 to 30 w m^2 cm^{-1} sr^{-1}. This increase in radiance appears to be driven primarily by the larger number of smaller particles present over the instruments although a thickening of the layer is also partially responsible.

Plates 1c, 1e and 1f show comparisons of the cloud properties derived from the radar-interferometer technique with results retrieved from geostationary satellite observations. The visible-infrared-solar-infrared (VIST) technique, described by *Minnis et al.* [1995] was used. The VIST technique, as applied here, uses data collected at 4 km resolution at channels centered at 0.65 μm, 3.9 μm, and 10.9 μm. The data are averaged over an area centered on the SGP site that extends 0.6° in latitude and 0.8° in longitude. The 0.65 μm radiance data were converted to reflectances as in the work of *Minnis and Smith* [1998]. The reflectance and emittance parameterizations described by *Minnis et al.* [1997] were used to retrieve the effective diameter, IWP, and visible optical depth. The effective diameters were converted to effective radius using the parameterization shown in Figure 1. The IWP comparison (Plate 1e) shows quite good agreement and captures well the evolving nature of the cirrus layer. The particle sizes retrieved from the satellite data, on the other hand, are consistently much smaller than retrieved by the radar-interferometer technique. Since the radar is most sensitive to the largest particles, while the VIST is more sensitive to smaller particles near cloud top, these results are not surprising. However, since the radar-interferometer algorithm allows for a bulk density that depends on the particle size (see Figure 2), the discrepancy may be partially explained by the difference in crystal density assumed by the two techniques; with particle sizes in the 90 μm range, we would infer a bulk density near 0.5 g m^{-3}, while the VIST algorithm assumes solid ice crystals. In essence the two retrieval algorithms sense the same amount of ice mass, but the algorithms distribute the mass differently.

It is evident from the preceding discussion that the radar-interferometer algorithm diagnoses subtle as well as substantial changes in the cloud microphysical properties. However, given the assumptions in the mathematical derivation of the algorithm, there is no guarantee that the retrieved properties are correct. As partial validation of the results, we therefore use the derived water path and effective size as input to the visible spectrum radiative parameterization of FL93 and then use the parameterized single scattering-properties of the layer as input to the radiation transfer model of *Toon et al.* [1989] as modified by *Kato et al.* [1997]. Plate 1f shows the visible optical depth of the cirrus layer. The close agreement between the optical depths derived from GOES data and those derived from the reflectivity-radiance algorithm is evident. During this case, the visible optical depth ranges from approximately 1 during the period when the layer was geometrically thin to about 3.5 during the maxima in IWP

Plate 1g shows the comparison between calculated and observed downwelling solar fluxes at the surface. These fluxes are expressed in terms of the fraction of the clear sky flux at the surface removed by the cloud layer. The clear sky fluxes were derived using the technique of *Long* [1996]. The close agreement between calculations and observations is evident. The overcast and rather uniform nature of this layer lends itself well to testing the validity of the retrieval in this way since the assumption of a plane parallel layer is reasonably approximated. The poorest agreement occurs near the end of the case (after 2200 UTC) when the solar zenith angles are becoming large (> 70°). However, even though the absolute agreement is poor, the trend of increasing cloud forcing is accurately characterized. The microphysical properties of the layer changed markedly from earlier periods with concentrations significantly higher and effective sizes somewhat smaller. It is possible that a region of active ice crystal generation was advecting over the site at this time and the retrieval algorithm captures the evolution of the cirrus layer. If our interpretation is correct, then it is equally likely that low-reflectivity regions near the actual cloud top were below the detection threshold of the radar, and the total ice mass in the column is underpredicted, while the effective size is overestimated [*Mace et al.*, 1998]. This is consistent with our overestimation of the solar transmittance during this period.

4. Summary and Future Work

In order to develop a continuous record of the characteristics of optically thin cirrus using the operational ARM data streams, we have developed a retrieval algorithm that uses layer-averaged radar reflectivity and observations of downwelling radiance observed by an interferometer to retrieve the layer-averaged microphysical properties in terms of an

assumed low-order modified gamma size distribution. This technique uses ideas similar to those presented by M92 and M94 except that we have reformulated the scheme in terms of the FL93 radiative parameterization and constructed the algorithm to use AERI-observed infrared spectra. The retrieval algorithm is incorporated into an iterative scheme based on the MODTRAN3 radiance algorithm that accounts for scattering of radiation by the surface and cloud layer. The sensitivity of the algorithm to input data (Figure 3) reveals that the retrieved parameters depend to a nearly equal degree on the IR radiance and radar reflectivity. Observational uncertainty leads to larger errors in optical depth and water content as the radar reflectivity and beam emittance increase. We used in situ data to validate the algorithm (Figure 4) and demonstrated good agreement between a retrieved particle size distribution and a distribution collected by the PMS 2DC probe on the NASA DC8 during the SUCCESS field exercise. We also presented a case study (Plate 1) from which we retrieved the microphysical properties and used these properties to calculate the downwelling solar fluxes. Comparisons with observed fluxes and comparison with cloud properties derived from GOES data showed good agreement. We have also conducted comparisons between results from the algorithm described in this study and the M92 technique [S. Y. Matrosov, personal communication, 1998]. Water contents, effective particle sizes and particle concentrations showed quite good agreement.

The April 5, 1996 case study is a fortuitous example of a uniform cirrus overcast and the comparison between observed and calculated solar fluxes provide an excellent means of examining the validity of the retrieval algorithm in this case. In other cases, however, this validation approach will present some difficulties. Cirrus clouds typically have much more spatial inhomogeneity than the April 5 case, and a point-by-point comparison of observed and calculated fluxes will provide only limited information. Such a case is examined by *Mace et al.* [1998] where event-averaged solar fluxes are compared and shown to provide reasonable agreement. Other sources of validation are also possible. To remove the ambiguity of plane parallel flux calculations, we require validation data sufficiently independent of the data used as input to the retrieval algorithm, and this validation data must sense some property of the zenith sky. For instance, we are investigating means of comparing computed and AERI-observed scattered solar radiances in the 3 μm atmospheric window region as well as comparing with solar radiances observed by the whole sky imager. We also plan to use the retrieved microphysical properties in a forward calculation of GOES and AVHRR solar and IR radiances. Comparison of optical depths derived from sun photometer, shadow band radiometer, and lidar data will also be used for validation when these products are available. It may also be possible to use some of these observations as additional input data to the retrieval algorithm. Applying confidence limits on data collected at night will be developed as we gain additional experience with daytime cases. From a radiative point of view, the only requirement for the night data is that they provide the correct downwelling and upwelling radiances. The downwelling radiance is guaranteed, and we will perform a forward calculation of the upwelling radiances for direct comparison to satellite measurements.

Preliminary calculations using data from the operational 8 mm radar at the SGP site are encouraging, and development of a long-term climatology of thin cirrus microphysical properties is ongoing. We are also developing algorithms that treat more general situations. The algorithm described in this paper as well as the techniques of M94 and M92 require optically thin cirrus with no lower clouds. Preliminary calculations with SGP radar data indicate that of all cirrus events, lower-level cloud layers were present 27, 29, and 36% of the time during April, May and June 1997, while this statistic was 58% for the Autumn 1994 data examined by Mace et al. [1997]. We are therefore developing algorithms that combine various data sources in order to increase the fraction of cirrus cases that have estimated microphysical properties.

Acknowledgements. This research benefited greatly from many useful discussions with Eugene Clothiaux of the Pennsylvania State University and Sergey Matrosov of the NOAA Environmental Technology Laboratory. The Pennsylvania State University 94 GHz radar was constructed by Robert Peters. Our appreciation is also extended to the personnel at the SGP ARM site for their assistance in collecting the data used in this study. This research was supported by the Environmental Science Division of the U. S. Department of Energy (grant DE-FG02-90ER61071) and NASA grants NAG-1-999 and NAG-5-2701, the U.S. Department of Energy interagency agreement DE-AI02-97ER62341, the NASA FIRE program, and the Earth Observing System Interdisciplinary Program, NASA/Office of Mission to Planet Earth through the Clouds and Earth Radiant Energy System Project.

References

Ackerman, T. P., K. N. Liou, F. P. Valero, and L. Pfister, Heating rates in tropical anvils. *J. Atmos. Sci.*, 45, 1606-1623, 1988.

Auer, A. H. Jr., and D. L. Veal, The dimension of ice crystals in natural clouds. *J. Atmos. Sci.*, 27, 919-926, 1970.

Atlas, D., S.Y. Matrosov, A.J. Heymsfield, M.-D. Chou, and D.B. Wolff, Radar and radiation properties of ice clouds. *J. Appl. Meteorol.*, 34, 2329-2345, 1995.

Berk, A., L. S. Bernstein, and D. C. Robertson, MODTRAN: A moderate resolution model for LOWTRAN7, Tech. Rep. GL-TR-89-0122, 38 pp., 1989 (Available from Geophys. Lab., Hanscom Air Force Base, Mass)

Brown, P. R. A., and P. N. Francis, Improved measurements of the ice water content in cirrus using a total water probe, *J. Atmos. Oceanic. Technol.*, 11, 410-414, 1995.

Clothiaux, E. E., M. A. Miller, B. A. Albrecht, T. P. Ackerman, J. Verlinde, D. M. Babb, R. M. Peters, and W. J. Syrett, An evaluation of a 94-GHz radar for remote sensing of cloud properties, *J. Atmos. Oceanic Technol.*, 12, 201-229, 1995.

Dowling, D. R., and L. F. Radke, A summary of the physical properties of cirrus clouds, *J. Appl. Meteorol., 29*, 970-978, 1990.

Ebert, E. E., J. A. Curry, A parameterization of ice cloud optical properties for climate models, *J. Geophys. Res,* 97, 3831-3836, 1992.

Fu, Q. and K.N. Liou, Parameterization of the radiative properties of cirrus clouds, *J. Atmos. Sci.*, 50, 2008-2025, 1993.

Gossard, E.E., Measurement of cloud droplet size spectra by Doppler radar, *J. Atmos. Oceanic Technol.*, 11, 712-726, 1994.

Kato, S., T. P. Ackerman, E. E. Clothiaux, J. H. Mather, G. G. Mace, M. L. Wesley, F. Murcray, and J. Michalsky Uncertainties in modeled and measured clear-sky surface shortwave irradiances, *J. Geophys. Res.*, 102, 25,881-25,898, 1997.

Liou, K. N., Influence of cirrus clouds on weather and climate: A global perspective, *Mon. Weather Rev.*, 114, 1167-1199 1986.

Lohmann, U., and E. Roeckner, Influence of cirrus cloud radiative forcing on climate and climate sensitivity in a general circulation model, *J. Geophys. Res.*, 100, 16305-16323, 1995.

Long, C.N., Surface radiative energy budget and cloud forcing: Results from TOGA COARE and techniques for identifying and calculating clear sky irradiance, 1995, Ph.D. thesis, The Penn. State University, Univ. Park, 193 pp.

Mace, G.G., D. O'C. Starr, T. P. Ackerman, and P. Minnis, Examination of coupling between an upper-troposphere cloud system and synoptic-scale dynamics diagnosed from wind profiler and radiosonde data, *J. Atmos. Sci.*, *52*, 4094-4127, 1995.

Mace, G.G., T.P. Ackerman, E.E. Clothiaux, and B.A. Albrecht, A study of composite cirrus morphology and its relationship to large-scale meteorology, *J. Geophys. Res.*, 102, 13,581-13,593, 1997.

Mace, G. G., S. Kinne, T. P. Ackerman, An examination of cirrus cloud characteristics using data from a millimeter wave radar and lidar: The 24 April SUCCESS case study. *Geophys. Res. Lett.*, 25, 1133-1136, 1998.

Matrosov, S.Y., T. Uttal, J.B. Snider, and R.A. Kropfli, Estimation of ice cloud parameters from ground-based infrared radiometer and radar measurements, *J. Geophys. Res.*, 97, 11567-11574, 1992.

Matrosov, S.Y., B.W. Orr, R.A. Kropfli, and J.B. Snider, Retrieval of vertical profiles of cirrus cloud microphysical parameters from Doppler radar and infrared radiometer measurements, *J. Appl. Meteor.*, 33, 617-626, 1994.

Minnis, P. and W. L. Smith Jr., Cloud and radiative fields derived from GOES 8 during SUCCESS and the ARM-UAV Spring 1996 flight series, *Geophys. Res. Lett.*, 25, 1125-1128, 1998.

Minnis, P., P. W. Heck and D. F. Young, Inference of cirrus cloud properties using satellite-observed visible and infrared radiances, II, Verification of theoretical cirrus radiative properties. *J. Atmos. Sci.*, 50, 1305-1322, 1993a.

Minnis, P., Y. Takano and K. -N. Liou, Inference of cirrus cloud properties using satellite-observed visible and infrared radiances, I, Parameterization of radiance fields, *J. Atmos. Sci.*, 50, 1279-1304, 1993b.

Minnis, P., D. P. Dratz, J. A. Coakley Jr., M. D. King, R. Arduini, D. P. Garger, P. W. Heck, S. Mayor, W. L. Smith Jr., and D. G. Young, Cloud optical property retrieval (Subsystem 4.3), in *Clouds and the Earth's Radiant Energy System (CERES) Algorithm Theoretcial Basis Document*, vol. 3: *Cloud Analyses and Radiance Inversions (Subsystem 4)*, edited by CERES Science Team, pp. 135-176, *NASA RP 1376*, 1995.

Minnis, P., D. P. Gerber, D. F. Young, R. F. Arduini, and Y. Takano, Parameterizations of reflectance and effective emittance for satellite remote sensing of cloud properties, *J. Atmos. Sci.*, in press, 1997.

Platt, C. M. R., and G. L. Stephens, The interpretation of remotely sensed high cloud emittance, *J. Atmos. Sci.*, 37, 2314-2322, 1980.

Ramaswany, V., and A. Detwiler, Interdependence of radiation and microphysics in cirrus clouds, *J. Atmos. Sci.*, 43, 2289-2301, 1986.

Schneider, T. L., and G. L. Stephens, Theoretical aspects of modeling backscattering by cirrus partilces at millimeter wavelengths, *J. Atmos. Sci.*, 52, 4367-4385, 1995.

Schroeder, J. A., and E. R. Westwater, Users' guide to WPL microwave radiative transfer software, *NOAA Tech. Memo., ERL WPL-213*, 84 pp., Environ. Technol. Lab., Boulder, Colo., 1991.

Smith, W. L., X. L. Ma, S. A. Ackerman, H. E. Revercomb, and R. O. Knuteson, Remote sensing cloud properties from high spectral resolution infrared observations, *J. Atmos. Sci.*, 50, 1708-1720, 1993.

Stamnes, K., S.-C. Tsay, W. J. Wiscombe, and K. Jayaweera, Numerically stable algorithm for discrete-ordinate-method radiation transfer in multiple scattering and emitting layered media, *Appl. Opt.*, 27, 2502-2509, 1988.

Starr, D. O'C., and D. P. Wylie, The 27-28 October 1986 FIRE cirrus case study: Meteorology and clouds, *Mon. Wea. Rev.*, 118, 2259-2287, 1990:.

Stephens, G. L., S.-C. Tsay, P. W. Stackhouse, and P. J. Flatau, The relevance of the microphysical and radiative properties of cirrus clouds to climate and climatic feedback, *J. Atmos. Sci.*, 47, 1742-1753, 1990.

Stokes, G. M., and S. E. Schwartz, The Atmospheric Radiation Measurement (ARM) Program: programmatic background and design of the cloud and radiation test bed, *Bull. Am. Meteorol. Soc.*, 75, 1201-1221, 1994.

Takano, Y., and K. N. Liou, Radiative transfer in cirrus clouds, I, Single-scattering and optical properties of hexagonal ice crystals, *J. Atmos. Sci.*, 46, 3-19, 1989.

Toon, O. B., C. P. McKay, T. P. Ackerman, and K. Santhanam, Rapid calculation of radiative heating rates and photodissociation rates in inhomogeneous multiple scattering atmospheres, *J. Geophys. Res.*, 94, 16,287-16,301, 1989.

Wylie, D. P., and W. P. Menzel, Two years of cloud cover statistics using VAS, *J. Clim.*, 2, 380-392, 1989.

G.G. Mace, Department of Meteorology, University of Utah, 819 Browning Bldg., Salt Lake City, UT 84112. (email:mace@atmos.met.utah.edu)

T. P. Ackerman, Department of Meteorology, The Pennsylvania State University, University Park, PA 16802.

P. Minnis and D. F. Young, Atmospheric Sciences Division, NASA Langley Research Center, Hampton, VA

(Received October 17, 1997; revised May 15, 1998; accepted May 27 1998.)